Energy 80 (2015) 567–574

Contents lists available at ScienceDirect

Energy

journal homepage: www.elsevier.com/locate/energy

The lazy greedy algorithm for power optimization of wind turbine positioning on complex terrain

M.X. Song [a], K. Chen [b], X. Zhang [c, *], J. Wang [a]

[a] Department of Control Science and Engineering, Tongji University, Shanghai 201804, PR China
[b] Key Laboratory of Enhanced Heat Transfer and Energy Conservation of the Ministry of Education, School of Chemistry and Chemical Engineering, South China University of Technology, Guangzhou 510640, Guangdong, PR China
[c] Key Laboratory for Thermal Science and Power Engineering of Ministry of Education, Department of Engineering Mechanics, Tsinghua University, Beijing 100084, PR China

ARTICLE INFO

Article history:
Received 27 June 2014
Received in revised form
30 October 2014
Accepted 4 December 2014
Available online 30 December 2014

Keywords:
Wind farm micro-siting
Wind turbine wake model
Submodular

ABSTRACT

Wind farm micro-siting is to determine the optimal positions of wind turbines within the wind farm, with the target of maximizing total power output or profit. This paper studies the performance of the lazy greedy algorithm on optimization of wind turbine positions above complex terrain. Instead of the traditional linear models, computational fluid dynamics and virtual particle wake flow model are employed in the present study for a more accurate evaluation of wind energy distribution and wind power output of wind farm on complex terrain. The validity of the submodular property used by the lazy greedy algorithm is discussed for the wind farm micro-siting optimization problem. By conducting the numerical tests, results demonstrate that the combination of the lazy greedy algorithm and the virtual particle wake model is effective in optimizing wind turbine positioning on complex terrain, for it produces better solution in less time comparing to the previous bionic method.

1. Introduction

Wind power generation is one of the clean and renewable energy sources with the most matured technologies of utilization. China is facing extreme energy and environment problem, which makes it urgent to develop highly efficient wind power generation technologies. To increase the power production efficiency of a wind farm, optimal designs of the wind turbines and the wind farm micro-siting are both important. This paper studies the wind farm micro-siting problem on complex terrain. Wind power generation efficiency is affected by the wind turbine layout in two ways. One is due to the non-uniform distribution of wind resources caused by the topography. Another is due to the velocity reduction caused by turbine wake flow. Therefore, the wind turbine layout must be carefully designed to reduce wake flow interaction and to increase total power output. In the past, much research has been carried out on the optimization of wind turbine layouts.

Among those approaches, the GA (genetic algorithm) is the most popular method. Mosetti, et al. [1] introduced GA to the wind farm micro-siting problem for the first time. In their paper, the wind farm area is discretized into Cartesian grids, and binary-coding is used to represent which grids have turbines installed. The installation cost is considered as a function only related to the total number of turbines. Their results demonstrate the effectiveness of GA in solving the wind farm micro-siting optimization problem. After that, many other models and optimization approaches have been studied for this problem. Albadi, et al. [2] studies the optimum tower height problem of wind turbines. An installation cost function which is linearly correlated with the tower height is used. Chen, et al. [3] did research on the optimization of wind turbine positioning with different hub heights using genetic algorithm, employing the similar linear cost function for wind turbine installation. González, et al. [4,5] used the NPV (Net Present Value) as a more realistic cost function, which includes the initial investment, the decommissioning, the present residual value, the financial benefit, and the ordinary operation and maintenance costs. Wan, et al. [6] used real-coding in GA, where turbines can be sited freely in the designated region, instead of being restricted to the grid nodes. These previous studies all indicate that GA is an effective approach for this problem. However, one of the disadvantages of GA is that it requires a large population and a huge number of generations of evolution. During its optimization process, millions of different wind turbine layouts emerges. Their power outputs and turbine wake flow effects all need to be evaluated, so that GA can eliminate worse solutions and retain better solutions. Therefore, in

* Corresponding author.
E-mail address: x-zhang@tsinghua.edu.cn (X. Zhang).

http://dx.doi.org/10.1016/j.energy.2014.12.012
0360-5442/

most of the studies using GA and similar algorithms, the linear model [7] is used to simulate wind turbine wake flow, which limits the approaches to be valid only for flat terrain. For complex terrain scenarios, non-uniform flow field distorts the turbine wake flow. Applying linear model to non-uniform flow field will bring additional error.

The virtual particle model has been developed in previous study [8] for simulating wind turbine wake flow effect in non-uniform flow field. This model reflects the characteristics of wake flow interactions much more realistic than the traditional linear model, and costs much less time than detailed numerical calculation on flow field around the turbine blades. It has already been validated in assessing wind power production [9]. Since the virtual particle model requires much longer time than the linear model, integrating it with GA would result in unacceptable time for engineering applications. Previous study has also introduced the bionic method to optimize the wind turbine layout [10]. The bionic method implements the concept of greedy algorithm. This method deals with only one turbine layout. In each step, it adds or moves one turbine to a better location that bring higher power output for the turbine. After several cycles of adding and moving turbines, the optimized solution is obtained. The bionic method requires much less times of conducting wake flow calculation, and can be integrated with the virtual particle model.

The lazy greedy algorithm, as a variation of the original greedy algorithm, has been introduced to the wind farm micro-siting optimization problem by Zhang et al. [11]. Their paper reveals that the problem has a so-called submodular property. With this property, the optimization process of greedy can be significantly simplified, saving much computation time. Terrain complexity has been considered in their study. However, the wake flow is simulated by a modified linear model, which takes the velocity direction at the turbine hub under consideration, but ignores the flow field non-uniformity in the downstream regions.

In the present study, the lazy greedy algorithm is integrated with CFD (computational fluid dynamics) and virtual particle wake flow model. In order to focus on discussing the validity and effectiveness of the submodular property and the lazy greedy algorithm, the present study only considers the optimization of power output of the wind farm. The combination produces a more accurate approach to optimize wind turbine layout on complex terrain. Numerical cases have been used for testing. Results show that the present method is effective in solving the wind farm micro-siting problem on complex terrain, for it not only obtains better solutions, but also takes much less time than the previous methods.

2. Wind power evaluation models

To develop an optimization method that produces wind turbine layout with high power output, it is essential to employ models that can accurately evaluates the power output of a wind farm according to given turbine layout. In present study, the evaluation is done in the following three steps: (1) The flow field of the empty layout (with no turbines, only the terrain topography) is numerically calculated using CFD. This calculation is carried out for only once. During the later optimization process, this flow field for empty layout maintains unchanged, providing the background flow field for wake flow simulation. (2) Simulate the turbine wake flow by using virtual particle model. The simulated effect is then superimposed to the background flow field, obtaining the wake influenced flow field. (3) Power output and turbine efficiencies can be calculated by introducing the turbine power curve model. The details of the models are stated in the following subsections.

2.1. Computational fluid dynamics

The optimization problem studied in this paper is for wind farm design before its construction. The instantaneous status of flow field is not interested. Therefore, the RANS (Reynolds Averaged Numerical Simulation) with standard k-ε model [12] is used to solve the steady Navier–Stokes equations. The governing equations are

$$\frac{\partial u_i}{\partial x_i} = 0 \tag{1}$$

$$\rho u_j \frac{\partial u_i}{\partial x_j} = -\frac{\partial p}{\partial x_i} + \frac{\partial}{\partial x_j}\left(\mu_t \frac{\partial u_i}{\partial x_j}\right) \tag{2}$$

$$\rho u_j \frac{\partial k}{\partial x_j} = \frac{\partial}{\partial x_j}\left(\frac{\mu_t}{\mathrm{Pr}_k}\frac{\partial k}{\partial x_j}\right) + \frac{\mu_t}{2}\left(\frac{\partial u_i}{\partial x_j} + \frac{\partial u_j}{\partial x_i}\right)^2 - \rho\varepsilon \tag{3}$$

$$\rho u_j \frac{\partial \varepsilon}{\partial x_j} = \frac{\partial}{\partial x_j}\left(\frac{\mu_t}{\mathrm{Pr}_\varepsilon}\frac{\partial \varepsilon}{\partial x_j}\right) + C_1\frac{\mu_t}{2}\left(\frac{\partial u_i}{\partial x_j} + \frac{\partial u_j}{\partial x_i}\right)^2\frac{\varepsilon}{k} - C_2\rho\frac{\varepsilon^2}{k} \tag{4}$$

where the turbulent viscosity is

$$\mu_t = \rho C_\mu \frac{k^2}{\varepsilon} \tag{5}$$

For the wind farm with large open space, the constants in the equations are chosen as: $C_1 = 1.44$, $C_2 = 1.92$, $\mathrm{Pr}_k = 1.0$, $\mathrm{Pr}_\varepsilon = 1.85$, $C_\mu = 0.033$ [13].

In applications, wind velocities on the surrounding borders are difficult to measure. One of the usual way is to couple the CFD calculation with meso-scale simulation, such as KAMM [14] or WRF [15] models. The present study concentrates on discussing the performance of optimization algorithms, the terrain is randomly generated by the diamond-square algorithm [16]. Generally, the typical exponential profile is used for boundary conditions, as listed below.

$$\begin{aligned} u(z) &= u_{\mathrm{ref}}\left(\frac{z}{z_{\mathrm{ref}}}\right)^\alpha \cos\theta \\ v(z) &= u_{\mathrm{ref}}\left(\frac{z}{z_{\mathrm{ref}}}\right)^\alpha \sin\theta \\ w(z) &= 0 \end{aligned} \tag{6}$$

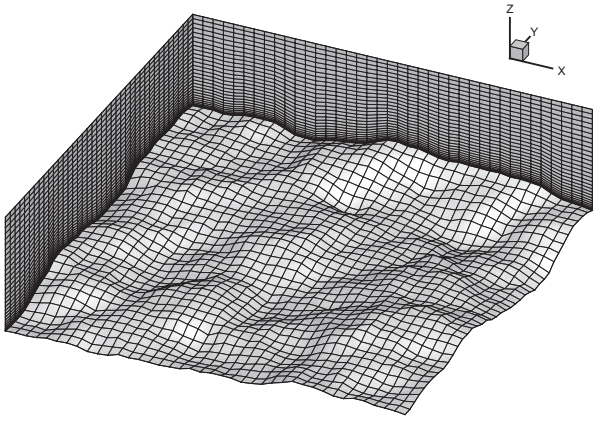

Fig. 1. The terrain following mesh and elevation.

where z is the height to the ground surface, u_{ref} is the reference wind speed at the reference height z_{ref} α is set to be 0.14 in the present study. And θ is the angle of incoming wind direction.

The calculation domain is discretized by the terrain-following mesh. The grids of the bottom layer are adapted to the ground surface, and the vertical grid lines are all perpendicular to the horizon. Fig. 1 is an example of the terrain-following mesh generated on a complex terrain, the present resolution is 40 × 40 × 30.

In the numerical study in this paper, the incoming wind is along the positive direction of the X axis, with $u_{ref} = 6$ m/s and $z_{ref} = 60$ m. Fig. 2 plots the calculated result of CFD in the surface 60 m above the ground, where filled contours show the magnitude of wind velocity, and curves with arrows are the stream lines. This flow field represents the initial wind energy distribution of the wind farm before turbines are installed. It will be used as the background flow field in the virtual particle wake flow model described in the next section.

2.2. Virtual particle wake flow model

The virtual particle model was previously presented to solve the problem that the traditional linear model is not valid in non-uniform flow field [8]. The linear model suggested by Katic [7] or other similar models assume that the wake influenced flow field can be considered as a background flow field (not influenced) plus a velocity decrement field caused by wake deficit, so that the calculation of velocity decrement caused by wake effect can be isolated from the entire flow field, treating the wake development as uncoupled with the airflow itself. The same basic idea is implemented in the virtual particle model. But unlike the linear model that treat the wake affected area as a conical region, the virtual particle model establishes the governing equation for the velocity decrement as if it was a kind of convective and diffusive matter. The equation is then solved numerically, whose result can be transformed to present the distribution of intensity of velocity decrement caused wake flow effect. The velocity decrement is superimposed to the background flow filed, obtaining the approximate wake influenced flow field. The details are explained below.

The approximate governing equation of the virtual wake flow matter is deduced as below. The momentum conservation equations from fluid dynamics before and after the turbine installation are both in the form of Navier–Stokes equations.

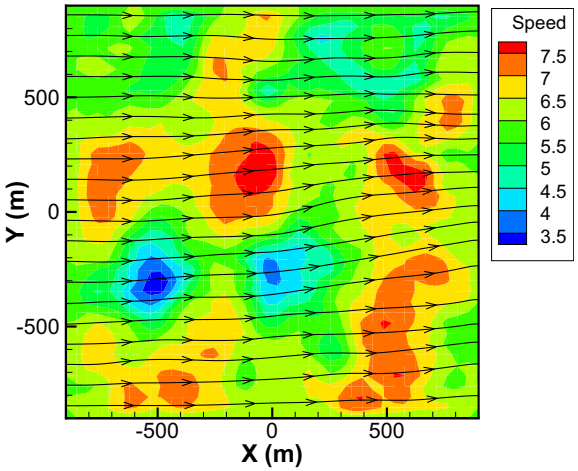

Fig. 2. Velocity distribution of the calculated flow field at height 60 m.

$$\rho u_j \frac{\partial u_i}{\partial x_j} = -\frac{\partial p}{\partial x_i} + \mu_t \frac{\partial^2 u_i}{\partial x_j \partial x_j} \tag{7}$$

$$\rho u'_j \frac{\partial u'_j}{\partial x_j} = -\frac{\partial p'}{\partial x_i} + \mu_t \frac{\partial^2 u'_i}{\partial x_j \partial x_j} \tag{8}$$

where the variables without and with primes are before and after wind turbine installation respectively. When linearizing the convective terms and ignoring the change of pressure caused by wake flow, subtracting Equation (8) from (7), it obtains

$$u_j \frac{\partial(\Delta u_i)}{\partial x_j} = \nu_t \frac{\partial^2(\Delta u_i)}{\partial x_j \partial x_j} \tag{9}$$

where $\Delta u_i = u_i - u'_i$, which is the velocity decrement caused by wake flow. Introducing a kind of virtual matter that has the concentration as Δu_i, Equation (9) becomes the governing equation of the development of the virtual matter. The boundary condition for this equation is the velocity decrement right behind the turbine hubs, which can be deduced according to the thrust coefficient of the wind turbine. With the equation deduced and the parameters determined, the equation can theoretically be numerically solved. However, the scale of wind farm is usually in the order of several kilometers, the grid size in CFD calculation cannot accurately resolve the shapes of the turbines and their rotating blades. In order to avoid additional difficulty of generating local refined mesh, the particle tracking method is introduced to simulate the convection and diffusion of the virtual matter.

Based on the background flow field solved by CFD without influences of wake flow, the particle tracking method runs a unsteady simulation of particle motions numerically. The each time step, particles are generated randomly in uniform probability within the rotation area of each turbine rotor. Each particle represents a small pack of velocity decrement to the grid where the particle is. More particles are generated within on step, more accurate the solution will be. In each time step, particles move convectively and diffusively. The local background velocity at the position of each particle is calculated by interpolating the background flow field. The convective motion of each particle is the local velocity of the background flow field multiplied by the temporal length of the step. The diffusive motion of each particle is simulated by adding Gaussian distributed random displacement to the position of the particle, which can be expressed by

$$\Delta x_d = \sigma_d \sqrt{-2 u r_r \Delta t \log R_1} \cos 2\pi R_2 \tag{10}$$

where σ_d is the diffusive coefficient, u is the local velocity of the background flow field, r_r is the radius of the turbine rotor, R_1 and R_2 are two independent random variable with uniform probabilities in Ref. [0,1]. When the particle generation and motion in each time step is done, the number of particles in each grid is counted, denoted as n, the relative concentration of the virtual matter, denoted as c, can be obtained by normalizing n with a standard number n_0:

$$c = \frac{n}{n_0}, \quad n_0 = \frac{\dot{n}}{u_0} \tag{11}$$

where $\dot{n}$ is the number of particles generated by one turbine in unit time, u_0 is the local velocity of the background flow field at the center of the turbine rotor. Assuming the velocity decrement is linearly correlated with the relative concentration of the virtual matter, the wake influenced velocity and any point within the domain can be calculated by

$$u' = u(1 - \beta c) \tag{12}$$

where β is the coefficient of linear transformation, which is related to the thrust coefficient of the turbine. For the wind turbine chosen for the present numerical study, the thrust coefficient is considered to be 0.88 as a constant, the same as in the references [1,10]. β has been determined in previous study [8] to be 0.65, corresponding to the thrust coefficient at 0.88.

With the nature of convection-diffusion equation, the affected area of wake flow can automatically adapt to local airflow, and is more reliably for complex terrain. The particle tracking method has been proved to be consistent with the standard convective and diffusive equation of scalar as in Equation (9) [17]. Refer to the previous paper [8] for the detailed steps and boundary conditions of performing the particle tracking.

Fig. 3 shows an example of wake flow simulation using virtual particle model. The simulated domain and terrain are the same as plotted in Fig. 1. Incoming wind is along the positive direction of the X axis. Incoming wind speed profile is exponential as expressed in Equation (6) with $u_{\text{ref}} = 6$ m/s, $z_{\text{ref}} = 60$ m, $\alpha = 0.14$. Three wind turbines are placed along the Y axis with spatial interval at 300 m. Tower height and rotor radius are 60 m and 20 m respectively. The figure plots the relative concentration c within the $Y = 0$ surface. Arrows in the figure stand for velocity vector field, while the filled contours are the relative concentration of the virtual matter. It is clearly seen that the virtual matter is concentrated at three positions where the turbine rotors exist. Since the virtual matter diffuses, the relative concentration decreases along the streamwise direction. Note that the region with higher concentration is distorted according to local airflow, indicating that the virtual particle model is able to resolve the wake flow in non-uniform flow field above complex terrain.

2.3. Turbine power curve

The power output of a wind turbine is determined by the incoming wind speed, the turbine mechanics design, and the control strategy. As a simplified analysis, the turbine power curve model is introduced to evaluate the averaged wind power output of a turbine. The characteristic properties of a turbine is the rated wind speed, the rated power output and the cut-out wind speed. Fig. 4 plots a typical turbine power curve.

For the turbine with power curve plotted in Fig. 4, the rated wind speed is 12.8 m/s, under which condition its power output is 630 kW (the rated power output). When incoming wind speed is lower than the rated speed, its power output is proportional to the incoming wind speed in the third order. Its cut-out wind speed is 25 m/s. Power output maintains the same when wind speed is in the range between the rated speed and the cut-out speed. For wind speed higher than the cut-out speed, turbine shuts down for safety, and power output drops to null.

In a wind farm with multiple wind turbines installed, as the wake influenced flow field is obtained by applying computational fluid dynamics and the virtual particle model, power output of each

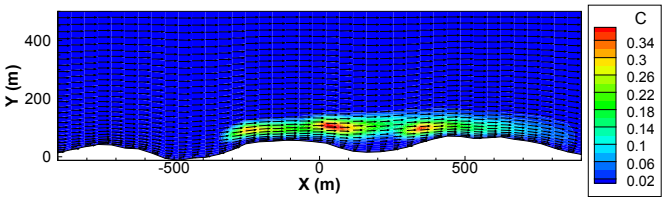

Fig. 3. Relative concentration of virtual wake flow matter above complex terrain.

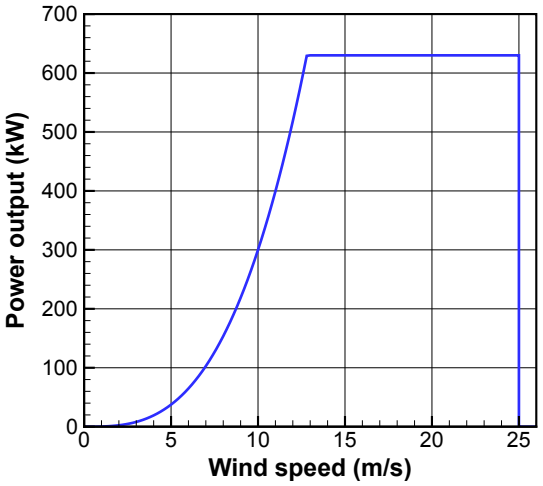

Fig. 4. A typical turbine power curve.

turbine can be calculated according to the power curve. Ignoring transmission loss, total power output of the wind farm is the sum of those of all the turbines.

3. Optimization approach

The present study intends to extend the lazy greedy algorithm to complex terrain scenarios. Comparing to previous study by Zhang et al. [11], the modified linear wake model is substituted by the present virtual particle model. According to previous study, the lazy greedy algorithm is valid when the problem has the submodular property. In order to apply the lazy greedy algorithm, it is necessary to discuss the submodular property for the present turbine layout optimization problem with virtual particle model.

3.1. Submodular property

An equivalent definition of the submodular property for the wind farm micro-siting optimization problem is as follows. Assume L is a finite set, whose elements represent all available positions in the wind farm for wind turbine installation. A is a subset of L, standing for a possible turbine layout. P is a function that calculates the total power output of a layout. For any $t \in L, t \notin A, s \in L, s \notin A, t \neq s$, if the following inequality holds, it is said that the problem is submodular.

$$P(A \cup \{s\}) - P(A) \geq P(A \cup \{t,s\}) - P(A \cup \{t\}) \tag{13}$$

The left side of the inequality is equal to

$$P_{s \leftarrow A \cup \{s\}} + \sum_{i \in A} (P_{i \leftarrow A \cup \{s\}} - P_{i \leftarrow A}) \tag{14}$$

The symbol $P_{i \leftarrow A}$ represents the power output of turbine i under the wake flow from turbines in layout A. The first term is the power output of turbine s when it is added to layout A. The summation term is the change of power output of existing turbines in layout A when turbine s is added. Similarly, the right side of Inequality 13 is equal to

$$P_{s \leftarrow A \cup \{t,s\}} + \sum_{i \in A} \left(P_{i \leftarrow A \cup \{t,s\}} - P_{i \leftarrow A \cup \{t\}}\right) + \left(P_{t \leftarrow A \cup \{t,s\}} - P_{t \leftarrow A \cup \{t\}}\right) \tag{15}$$

The first term is the power output of turbine s when it is added to layout $A \cup \{t\}$. Because turbine s may receive wake effect from

turbine t, it can be concluded that $P_{s\leftarrow A\cup\{s\}} \geq P_{s\leftarrow A\cup\{t,s\}}$. The last term in Equation (15) is the change of power output of turbine t when turbine s is added. Since turbine t may receive wake effect from turbine s, this term is not positive. As for the summation terms, the relation differs for different cases.

Take one turbine $a \in A$ as an example. As shown in Fig. 5 (a), $P_{a\leftarrow A\cup\{s\}} - P_{a\leftarrow A}$ represents the power loss of turbine a caused by wake flow from turbine s. If wake flow from turbine t does not affect turbine a, as shown in Fig. 5(b), the power loss of turbine a caused by wake flow from turbine s is identical to the case in Fig. 5(a), that is $P_{a\leftarrow A\cup\{s\}} - P_{a\leftarrow A} = P_{a\leftarrow A\cup\{t,s\}} - P_{a\leftarrow A\cup\{t\}}$. In this type of case, Inequality 13 holds, the problem is submodular. If wake flow from turbine t affects turbine a, as shown in Fig. 5(c), since the turbine power curve is a convex function for wind speed lower than the rated speed, the power loss of turbine a caused by wake flow from turbine s is less significant comparing to the case in Fig. 3(a). In this case $P_{a\leftarrow A\cup\{s\}} - P_{a\leftarrow A} < P_{a\leftarrow A\cup\{t,s\}} - P_{a\leftarrow A\cup\{t\}}$. It is not guaranteed that the problem is submodular.

A typical configuration is designed to study the validity of the submodular inequality for the cases above. In this configuration, incoming wind is along the positive direction of the X axis. Turbine a is fixed at (100 m,0 m), turbine s is initially located at (−100 m,−30 m), and turbine t is initially located at (−50 m,30 m). For this layout, the order of turbines from upstream to downstream is s, then t, and then a. The layout is plotted in Fig. 6.

Firstly, fix turbine s at its initial position (−100 m,−30 m), and let turbine t moves perpendicular to the airflow along the $X = -50$ m line. For different positions of turbine t, the terms in the submodular inequality are calculated. As plotted in Fig. 7(a), the red (in web version) curve denoted as *left* is the value of $P(\{a,s\}) - P(\{a\})$, while the blue (in web version) curve denoted as *right* is the value of $P(\{a,t,s\}) - P(\{a,t\})$. When $Y_t \leq -80$m or $Y_t \geq 50$m, turbine t is far away from the other turbines, the wake effect caused by turbine t can be ignored, which matched the situation in Fig. 5(b). When Y_t is between −70 m and 0 m, turbine t itself is highly influenced by turbine s, therefore the right side of the submodular inequality is smaller than the left side, the submodular inequality holds. When Y_t is between 10 m and 40 m, the right side exceeds the left side, the submodular inequality does not hold in this situation.

Secondly, fix turbine t at its initial position (−50 m,30 m), and let turbine s moves perpendicular to the airflow along the $X = -100$ m line. The results are plotted in Fig. 7(b). Similarly, when $Y_s \leq -70$ m or $Y_s \geq 90$ m, turbine s is far away from the other turbines. Wake flow generated by turbine s does not affect other turbines. Therefore the left side and the right side of the submodular inequality are equal. The submodular inequality does not hold when Y_s is between −60 m and −10 m.

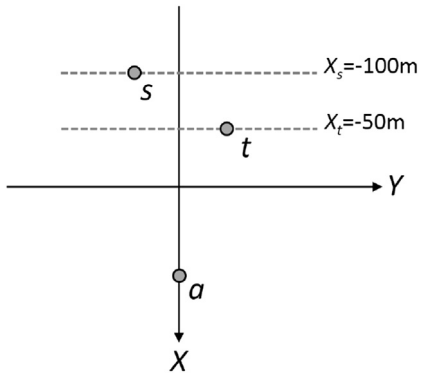

Fig. 6. Turbine layout of the typical configuration for studying submodular property.

According to the analysis above, for the three-turbine configuration, it can be concluded that: (1) The submodular inequality holds when one turbine is far away from the other two. In the case, any turbine receives wake flow from at most one other turbine. (2) When the three turbines are close to each other, making one turbine may receive wake flow from both the other turbines, the submodular inequality still holds for more situations. (3) Even when the submodular inequality does not hold, the maximum divergence is only 4.98 kW as appears when $Y_t = 20$ m. The property can still make it possible for the lazy greedy algorithm to work effectively. The numerical study in this paper demonstrates its effectiveness.

3.2. Optimization steps

The steps for the lazy greedy algorithm to optimize wind turbine layout is similar as in Zhangs paper [11], as listed below.

Step 1: Discretize the wind farm designated area into multiple scatter points, each one of which represents an available location for wind turbine installation.
Step 2: Give each point an evaluation value, which equals to the power increment of the wind farm if a new turbine is added at this point. When no turbine is sited, the evaluation values can be calculated directly from the flow field.
Step 3: Sort the points by their evaluation values in descending order.
Step 4: Add one turbine at the first point, who has the highest evaluation value. Remove the located point from the available point set.
Step 5: Test adding one turbine at the first point, apply the virtual particle wake model, calculate the power output of the wind farm, then update the evaluation value of this point.

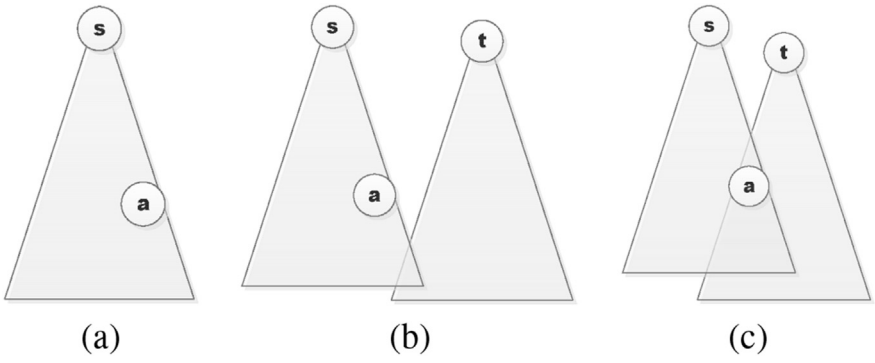

Fig. 5. Possible cases for discussing the submodular property, where wind blows from up to bottom.

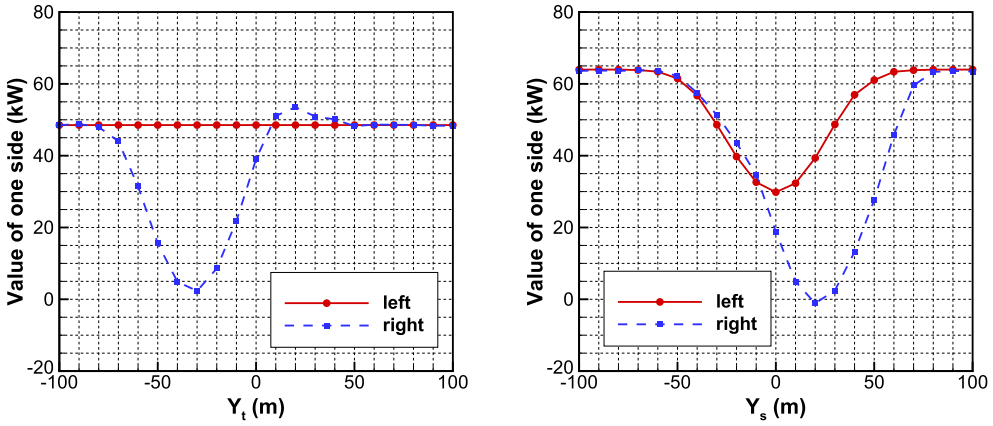

(a) turbine t moves along $X = -50$m (b) turbine s moves along $X = -100$m

Fig. 7. Value of the sides of the submodular inequality.

Step 6: If the updated evaluation value is still the highest one among all the available points, then confirm the adding. Otherwise, cancel the adding, resort the points by their evaluation values in descending order, go to Step 4.

Unlike the original greedy algorithm, the lazy greedy algorithm does not need to test all available points in order to find the optimal one. Benefiting from the submodular property, the updated evaluation value is always lower than the original one. Therefore, if the updated evaluation value is still higher than the others, it is guaranteed to be the really highest one. The testing stage can be significantly simplified. In the early steps of the optimization cycles, there is enough space for newly added turbines not to have wake flow interaction with existing turbines. This optimization method takes full advantages of the submodular property, and the optimization is extremely accelerated. But in the later steps, as the newly added turbine are inevitable to affect existing turbines, situations like the one in Fig. 5(c) emerges. The testing stage in each cycle of optimization may end up with a point that is not really the one with highest evaluation value. From this perspective, the lazy greedy algorithm for this specific problem is not exactly equivalent to the original greedy algorithm. However, it saves much computation time, which is its advantages for application of wind engineering.

4. Case study

In this section, a simple case is introduced to test the present optimization method. Wind farm is in a 2000 m × 2000 m square area, with terrain elevation and mesh plotted in Fig. 1. Incoming wind is along the positive direction of the x-axis. Boundary velocity is specified according the exponential profile as described in Equation (6), with reference wind speed $u_{\mathrm{ref}} = 6$ m/s at the reference height $z_{\mathrm{ref}} = 60$ m. Number of grids used for CFD calculation is $40 \times 40 \times 30$. The hub height of the wind turbines is 60 m, and the rotor radius is 20 m. The power curve of the chosen turbines is the same as plotted in Fig. 4. In the optimization, the number of turbines is fixed at 20.

The problem is optimized using the previous bionic method and the present lazy greedy method respectively. Grid number for optimization is 20 × 20. The results are plotted in Figs. 8 and 9.

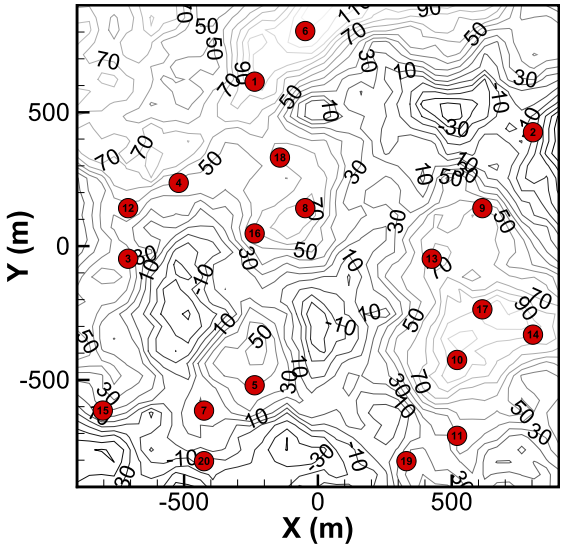

Fig. 8. Optimized turbine layout using bionic method.

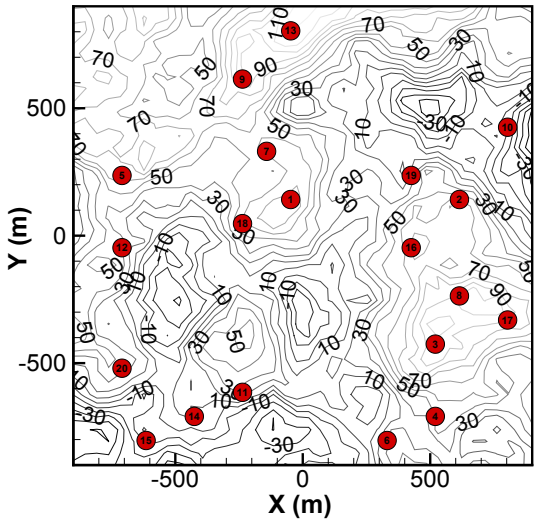

Fig. 9. Optimized turbine layout using lazy greedy method.

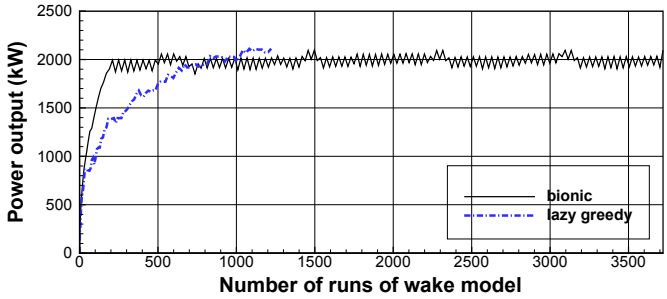

Fig. 10. Power output of wind farm during the optimization process with 20 × 20 grids.

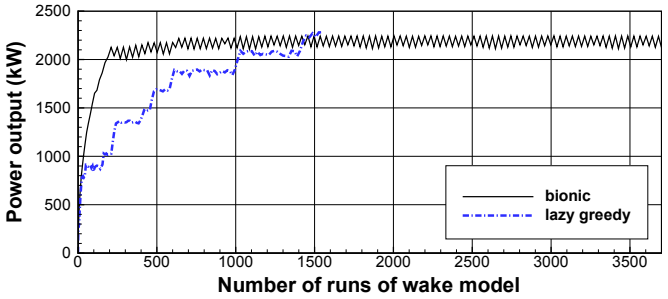

Fig. 12. Power output of wind farm during the optimization process with 40 × 40 grids.

The change of power output during the optimization process is plotted in Fig. 10. Since computational time may change on different computers, we use the number of runs of the wake flow model as an index of the time cost, denoted as N_w. The performed bionic optimization includes 20 steps of adding turbine stage and 180 steps of adjusting stage. N_w for the bionic optimization is 3720. The best solution emerges when N_w is 1497, with power output at 2095.77 kW. The lazy greedy method obtains final result when N_w is 1222, which is only about one third of the time cost of the bionic method. The obtained layout has power output at 2111.75 kW, which is higher than that of the bionic method.

The bionic method is essentially an accelerated and approximated greedy method with selfish evaluation function. In each optimization step during the bionic optimization, the only consideration for choosing location for the new turbine is its own power output, disregarding the influences to existing turbines. This strategy is very easy to implement, and cost less time in choosing the location for the new turbine. Meanwhile, the lazy greedy method have to test multiple locations in order to find an optimal one for the overall power output, it takes longer time to reach the same power output as the bionic method. However, when the number of turbines reaches the specified limit, the bionic method begins to adjust the turbine locations one by one, in the hope that a better layout may emerge. This stage is inefficient. It may runs into a loop, or runs for a extremely long time that approximates the enumerative algorithm.

Fig. 11 and Fig. 12 plots the power change during the optimization processes when grid resolution is 10 × 10 and 40 × 40 respectively. For the 10 × 10 grids, the bionic optimization runs for 200 steps, with total N_w at 3720. The best solution emerges when N_w is 2472, with power output at 1798.21 kW. The lazy greedy algorithm obtains its result when N_w is 1322, with power output at 1840.15 kW.

For the 40 × 40 grids, the bionic optimization follows the same process and runs for 200 steps with total N_w at 3720. The best solution emerges when N_w is 2199, with power output at 2244.48 kW. The lazy greedy algorithm obtains its optimized solution when N_w is 1547, with power output at 2281.09 kW.

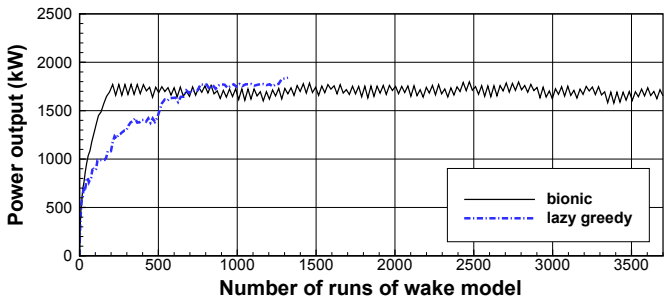

Fig. 11. Power output of wind farm during the optimization process with 10 × 10 grids.

Table 1
The best solutions obtained by the optimization processes.

	Power output (kW)	N_w
Bionic 10 × 10	1798.21	2472
Lazy 10 × 10	1840.15	1322
Bionic 20 × 20	2095.77	1497
Lazy 20 × 20	2111.75	1222
Bionic 40 × 40	2244.48	2199
Lazy 40 × 40	2281.09	1547

The results for the three different grid resolutions are listed in Table 1. Since the grid resolution of the flow field is 40 × 40 on the horizontal direction, grids finer than 40 × 40 for optimization will be based on interpolated velocities, which will not provide meaningful information about the details of wind resource distribution. According to the numerical results with different grid resolutions of optimization, the bionic method increases power output faster at the beginning of the optimization process. But from the perspective of the final outcome, the lazy greedy algorithm always produce better solution in shorter time. It can be concluded that the lazy greedy algorithm is effective in optimizing wind turbine layout on complex terrain. Generally, it has better performance than the previous bionic method. The increase of grid resolution in optimization enlarges the solution space, therefore better solution may be found with more grids.

5. Conclusion

The more efficient lazy greedy algorithm for wind farm micro-siting optimization is studied. By integrating computational fluid dynamics for wind energy assessment, and the virtual particle model for turbine wake flow simulation, the application of the lazy greedy algorithm is extended to the scenarios with complex terrains. The lazy greedy algorithm takes advantage of the submodular property of the optimization problem, which results in acceleration of the optimization process. The validity of the submodular property for the wind turbine positioning optimization problem is discussed. The analysis concludes that the submodular inequality does not hold only for a small portion of situations when multiple wake flows are influencing one turbine. Numerical case with complex terrain is used to test the present method. Results show that the present method is able to find better solution in less time than the previous bionic method. Even if the submodular property is not strictly correct for all the

cases, the lazy greedy algorithm is still effective for optimizing wind turbine layout in non-uniform flow field above complex terrain.

Acknowledgment

This research is supported by: the Program of International S&T Cooperation of China (2011DFG13020), China Postdoctoral Science Foundation (2013M530043), and the National High-Tech R&D Program (863 Program) of China (2007AA05Z426).

Nomenclature

Symbol

c	relative concentration of the virtual wake matter, 1
ε	turbulence dissipation rate, m^2/s^3
k	turbulent kinetic energy, m^2/s^2
μ_t	dynamic viscosity, kg/(m s)
N_w	number of runs of the wake flow model during optimization, 1
n	number of particles in each grid, 1
n_0	standard number of particles in a grid, 1
$\dot{n}$	particle generation rate, 1/s
P	function that calculates the power output of a wind farm, kW
p	pressure of the background flow field, N/m^2
p'	pressure of the wake influenced flow field, N/m^2
R_1, R_2	random variable uniformly distributed on [0,1], 1
r_r	radius of turbine rotor, m
ρ	density of air, kg/m^3
θ	angle of incoming wind direction, 1
u_0	wind speed at the center of a turbine rotor, m/s
u_i, u_j or u, v, w	velocity component of the background flow field, m/s
u_i'or u_j'	velocity component of the wake influenced flow field, m/s
Δu_i	decrement of velocity component caused by wake flow, m/s
u_{ref}	reference wind speed, m/s
x_i, x_j or x, y, z	coordinate, m
Δx_d	diffusive displacement of a particle within one time step, m
z_{ref}	reference height above the ground, m

References

[1] Mosetti G, Poloni C, Diviacco B. Optimization of wind turbine positioning in large windfarms by means of a genetic algorithm. J Wind Eng Ind Aerodyn 1994;51:105–16.
[2] Albadi MH, El-Saadany EF. Optimum turbine-site matching. Energy 2010;35:3593–602.
[3] Chen Y, Li H, Jin K, Song Q. Wind farm layout optimization using genetic algorithm with different hub height wind turbines. Energy Convers Manag 2013;70:56–65.
[4] González JS, Rodríguez AGG, Mora JC, Payán MB, Santos JR. Overall design optimization of wind farms. Renew Energy 2011;36:1973–82.
[5] González JS, Rodriguez AGG, Mora JC, Santos JR, Payan MB. Optimization of wind farm turbines layout using an evolutive algorithm. Renew Energy 2010;35:1671–81.
[6] Wan C, Wang J, Yang G, Zhang X. Optimal siting of wind turbines using real-coded genetic algorithms. In: European Wind Energy Association Conference and Exhibition, Marseille, France; 2009.
[7] Katic I, Højstrup J, Jensen NO. A simple model for cluster efficiency. In: European Wind Energy Association Conference and Exhibition, Rome, Italy; 1986. p. 407–10.
[8] Song MX, Chen K, He ZY, Zhang X. Wake flow model of wind turbine using particle simulation. Renew Energy 2012;41:185–90.
[9] Wu B, Song M, Chen K, He Z, Zhang X. Wind power prediction system for wind farm based on auto regressive statistical model and physical model. J Renew Sustain Energy 2014;6:013101.
[10] Song MX, Chen K, He ZY, Zhang X. Bionic optimization for micro-siting of wind farm on complex terrain. Renew Energy 2013;50:551–7.
[11] Zhang C, Hou G, Wang J. A fast algorithm based on the submodular property for optimization of wind turbine positioning. Renew Energy 2011;36:2951–8.
[12] Launder BE, Spalding DB. The numerical computation of turbulent flows. Comput Methods Appl Mech Eng 1974;3(2):269–89.
[13] Palma JMLM, Castro FA, Ribeiro LF, Rodrigues AH, Pinto AP. Linear and nonlinear models in wind resource assessment and wind turbine micro-siting in complex terrain. J Wind Eng Ind Aerodyn 2008;96:2308–26.
[14] Frank HP, Rathmann O, Mortensen NG, Landberg L. The numerical wind atlas – the KAMM/WAsP method. Tech. Rep. Roskilde, Denmark: Risø National Laboratory; 2001.
[15] Skamarock WC, Klemp JB, Dudhia J, Gill DO, Barker DM, Duda MG, et al. A description of the advanced research WRF version 3. Tech. Rep. Boulder, Colorado, USA: National Center for Atmospheric Research; 2008.
[16] Fournier A, Fussell D, Carpenter L. Computer rendering of stochastic models. Commun ACM 1982;25(6):371–84.
[17] Chen K, Song MX, Zhang X. The random walking method for steady linear convection-diffusion equation with axisymmetric disc boundary. Sci China Technol Sci 2014;57(4):804–10.